

Adhesion Energy of Phosphorene on different pristine and oxidized metallic substrates

Matteo Vezzelli^a, Carsten Gachot^b, Maria Clelia Righi^a

^aDepartment of Physics and Astronomy, University of Bologna, Bologna, 40127, Italy

^bInstitute of Engineering Design and Product Development, TU Wien, Wien, 1060, Austria

Abstract

Black phosphorus and its single-layer constituent, phosphorene, have emerged as promising two-dimensional materials with remarkable tribological properties. However, recent experimental investigations reveal complex substrate-dependent behavior that affects their lubricating capabilities. This computational study employs density functional theory calculations to quantify the adhesion energy of both pristine and oxidized phosphorene monolayers on various metallic substrates (aluminum, copper, iron, and chromium) and their corresponding oxides (Al_2O_3 , Cu_2O , Fe_2O_3 , and Cr_2O_3), correlating these fundamental interactions with experimentally observed tribological performance. Results demonstrate that oxidized phosphorene exhibits greater stability than its pristine counterpart and shows higher adhesion to all substrates, attributed to favorable interactions between oxygen non-bonding states and substrate empty states. Adhesion is systematically more favorable on pristine metals than on their corresponding oxides, with chromium and iron showing particularly strong interactions due to partially filled 3d orbitals. This result is consistent with the coefficient of friction decrease observed in tribological experiments after scratching the substrate, thus removing the outermost oxide layer. Charge redistribution and electronic structure analyses reveal system-dependent interfacial bonding characteristics, with some configurations inducing metallic character in phosphorene. These findings provide fundamental insights into substrate-dependent black phosphorus lubricating properties, highlighting the key role of layer-substrate adhesion.

Keywords: Black Phosphorus, Phosphorene, Adhesion Energy, Interfaces, Density Functional Theory, Tribology, Solid Lubricant

1. Introduction

Black phosphorus (BP), the most stable crystalline allotrope of phosphorus, has emerged as one of the most promising two-dimensional (2D) materials since its rediscovery as a monolayer system in 2014. This material has joined the expanding family of post-graphene 2D materials, which includes transition metal dichalcogenides, hexagonal boron nitride, and MXenes [1, 2].

Phosphorene, defined as a single layer exfoliated from bulk BP, represents a particularly important member of this material class. Its unique electronic properties have attracted considerable attention, particularly its direct bandgap of 0.3 eV [3, 4], which can be systematically tuned by varying the number of layers [5] or applying in-plane strain [6]. Beyond its electronic characteristics, phosphorene exhibits remarkable mechanical and tribological properties attributed to its anisotropic Young's modulus [7] and its exceptional ability to achieve ultralow friction when employed as a lubricant additive in aqueous solutions [8].

The superior tribological performance of phosphorene as both filler and composite material [8, 9, 10, 11] originates from the ability to reduce the surface energy of the substrate [12, 13] and the weak van der Waals interactions between layers [14, 15], which facilitate interlayer sliding and reduce friction. However, recent experimental investigations have revealed that BP's solid lubrication performance exhibits complex substrate-dependent behavior that challenges conventional assumptions about its lubricating capabilities [16].

From a structural perspective, BP possesses a distinctive atomic arrangement that governs its tribological properties. Each phosphorus atom contains five valence electrons in a $3s^23p^3$ configuration, forming four sp^3 hybridized orbitals. Three orbitals participate in bonding with adjacent phosphorus atoms, while the fourth hosts a lone electron pair, resulting

in a tetrahedral geometry that produces a characteristic puckered honeycomb lattice structure. This arrangement exhibits pronounced structural anisotropy: the material displays *zigzag* and *armchair* configurations along the x - and y -directions, respectively, while exhibiting a hexagonal structure along the z -direction. Each phosphorene layer comprises two atomic sub-layers connected by two distinct types of P-P bonds: intra-planar bonds within each sub-layer and weaker inter-planar bonds between sub-layers, as illustrated in the Supplementary Material [17, 18, 19, 20, 21].

The weak interlayer van der Waals interactions enable the mechanical exfoliation of bulk BP into few-layer or monolayer structures, analogous to the well-established exfoliation of graphite to produce graphene. However, these reduced-dimensional BP structures suffer from intrinsic instability [22, 23] and consequently exhibit high reactivity toward oxygen, moisture, and light [24, 25, 26, 27, 28, 29]. Paradoxically, the formation of phosphorus oxides resulting from BP degradation has been demonstrated to enhance friction and wear performance, as observed in atomic force microscopy (AFM) experiments [30] and when BP nanoflakes are incorporated as solid fillers in polytetrafluoroethylene (PTFE) [31]. Consequently, this computational study investigates both pristine and oxidized phosphorene monolayers, as depicted in Figure 1.

The substrate-dependent tribological behavior of BP was systematically investigated in the study "A Different Perspective on the Solid Lubrication Performance of Black Phosphorus: Friend or Foe?" [16], which demonstrated that BP's performance varies significantly with substrate material and contact conditions. That work identified adhesion between BP and the substrate as a critical factor determining its effectiveness as a solid lubricant. Building upon these experimental findings, the present computational study extends this analysis by quantifying

the adhesion energy of BP on identical metal substrates (steel, aluminum, copper, and iron) through density functional theory (DFT) calculations.

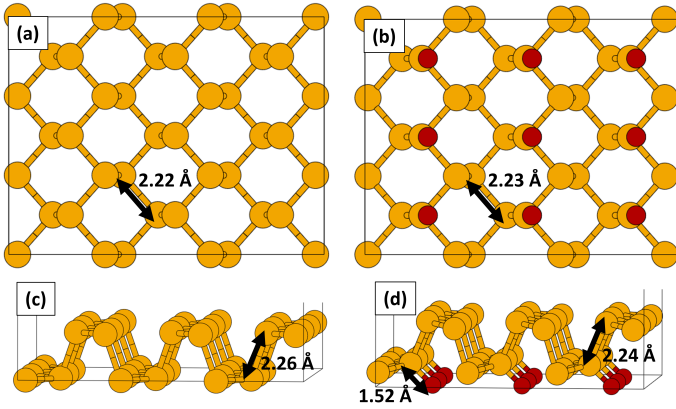


Figure 1: Comparison between pristine and oxidized phosphorene structures. (a) Bottom view and (c) side view of pristine phosphorene. (b) Bottom view and (d) side view of oxidized phosphorene with 25% of oxygen coverage.

The computational modeling focuses on the most stable crystallographic surfaces of the metal substrates examined in the experimental investigations. Additionally, the study considers the primary oxide phases for each metal. Pristine aluminum naturally develops a protective Al_2O_3 (alumina) passivation layer that prevents further oxidation [32], while on steel and iron surfaces, Fe_2O_3 (hematite) represents the predominant oxide phase [33, 34, 35, 36]. For copper, Cu_2O (cuprite) constitutes the primary oxide at temperatures up to 300°C , consistent with the experimental conditions employed in the referenced tribological tests [16, 37, 38]. The analysis additionally incorporates Cr_2O_3 (chromia) to account for the thin oxide layer that naturally forms on the chromium-bearing steel (AISI 52100) utilized in the experimental studies [39, 40].

This computational investigation aims to provide quantitative insights into the substrate-dependent adhesion behavior of BP, thereby elucidating the fundamental mechanisms underlying its variable tribological performance across different material systems.

2. Computational details

In this study, spin-polarized DFT calculations were performed following the plane-wave and pseudopotential approach as implemented in Quantum Espresso software [41]. The electronic wave functions were expanded on a plane-wave basis set, with ultrasoft pseudopotentials employed to describe the ionic species, including the core electrons [42]. The Generalized Gradient Approximation (GGA) within the Perdew-Burke-Ernzerhof (PBE) parameterizations was used as the exchange-correlation functional [43]. A Gaussian smearing of 0.005 Ry was employed to better describe the occupations of the electronic states around the Fermi level. Optimizations were carried out using the BFGS algorithm [44] and stopped when the total energy and forces converged below the threshold of 10^{-4} Ry and 10^{-3} Ry/Bohr, respectively. The convergence criteria for the self-consistent electronic (SCF) loop were set to 10^{-6} Ry. For every system considered, the kinetic energy cut-off to expand the wave function and the charge densities were set to 50 Ry and 400 Ry, respectively. All systems were constructed with at least 15 \AA of vacuum between vertical replicas.

The sampling of the Brillouin zone was performed without the inclusion of the Γ -point, using an appropriately converged Monkhorst-Pack grid of K-points, ensuring a total energy accuracy within 1 meV/atom compared to calculations with a denser grid. Equivalent reduced grids were employed to sample the corresponding most stable surfaces.

London dispersion forces were accounted for by adopting the D2 scheme [45], using 0.75 for the s6 scaling factor as suggested in the original paper. This dispersion scheme has yielded very good results for computing properties of BP and phosphorene interlayer energy [46].

Since DFT faces significant difficulties in accurately modeling the electronic structure and magnetic properties of transition-metal oxides, the DFT+U method was employed to better capture the strong localization of the d orbitals in these systems, accounting for the on-site Coulomb interactions [47]. The Hubbard parameters were determined empirically, with iterative adjustments made to optimize structural parameters and band gap values, ensuring an accurate description of the transition-metal oxides. The values used were 4.8 eV for the 3d orbitals of Fe_2O_3 , 7.0 eV for the 3d orbitals of Cr_2O_3 , and 11.0 eV for the 3d and 2p orbitals of Cu_2O . The Hubbard plots for the bulk materials are shown in the Supplementary Material.

Table 1 presents a comprehensive overview of the computational details used for bulk and substrate calculations. It includes the optimized bulk lattice parameters, calculated surface energies corresponding to the most stable surfaces and terminations, and the number of substrate layers used.

The optimized structural parameters and surface energies obtained in this study were validated against literature data. For pristine phosphorene, the calculated lattice parameters and surface energy are consistent with ref. [48]. The surface energies of Al(111), Cu(111), and Fe(110) agree with previous DFT calculations [49, 50, 51]. For $\text{Al}_2\text{O}_3(0001)$, both Al-terminated and O-terminated configurations were benchmarked against refs. [52, 53, 54]. The $\text{Cu}_2\text{O}(111)$ O-terminated surface structure and energetics are consistent with refs. [55, 56, 57], while $\text{Fe}_2\text{O}_3(0001)$ Fe-terminated and O-terminated surfaces were compared with refs. [36, 58, 59]. The Cr(110) surface energy matches literature values [49, 51], and $\text{Cr}_2\text{O}_3(0001)$ Cr-terminated surface with refs. [54, 59, 60]. The number of layers for each substrate ensures surface energy convergence as reported in the corresponding references.

For this study, calculations focused solely on monolayer phosphorene, as the primary interest was in determining adhesion energy. This approach optimized computational efficiency and resource utilization. Notably, other computational studies have employed bilayer phosphorus models only when investigating metal interfaces [21] or conducting molecular dynamics (MD) simulations [18].

For oxidized phosphorene, the bulk structure was constructed by replicating the most stable oxidized monolayer configuration along the out-of-plane direction. The bulk total energy (E_{bulk}) used in Equation 1 for surface energy calculations was obtained from this multilayer oxidized structure, ensuring consistency with the oxidation pattern of the monolayer system.

The $\text{Cr}_2\text{O}_3(0001)$ surface was chosen for the calculations, although the (1012) surface is more stable [54]. This choice was driven by computational constraints, as constructing a supercell with the (1012) surface would have required an extremely large model size. The (0001) surface, being the second in order of stability, was found to be an acceptable approximation, additionally

Material	Bulk cell	a (Å)	b (Å)	c (Å)	Surface cell	Surface plane	Surface energy (J/m ²)	n. of layers
Ph	orthorhom.	3.33	4.33	10.49	orthorhom.	[001]	0.18	1
Ph-ox	orthorhom.	3.33	4.33	10.49	orthorhom.	[001]	0.12	1
Al	cubic FCC	4.02	4.02	4.02	hexagonal	[111]	0.75	4
Al ₂ O ₃ Al-term	hexagonal	4.79	4.79	13.03	hexagonal	[0001]	2.11	6
Al ₂ O ₃ O-term	hexagonal	4.79	4.79	13.03	hexagonal	[0001]	3.83	6
Cu	cubic FCC	3.59	3.59	3.59	hexagonal	[111]	1.04	4
Cu ₂ O O-term	cubic	4.33	4.33	4.33	hexagonal	[111]	1.15	5
Fe	cubic BCC	2.84	2.84	2.84	primitive	[110]	2.33	3
Fe ₂ O ₃ Fe-term	hexagonal	5.11	5.11	13.76	hexagonal	[0001]	1.30	6
Fe ₂ O ₃ O-term	hexagonal	5.11	5.11	13.76	hexagonal	[0001]	2.36	6
Cr	cubic BCC	2.82	2.82	2.82	primitive	[110]	3.60	3
Cr ₂ O ₃ Cr-term	hexagonal	5.15	5.15	13.63	hexagonal	[0001]	1.57	6

Table 1: Optimized parameters for bulk and substrate calculations, where a , b , and c refer to the bulk lattice vectors. Abbreviations: Ph, phosphorene; Ph-ox, oxidized phosphorene.

Material	Phosphorene (pristine and oxidized)			Substrate		
	Supercell	Mismatch on a	Mismatch on b	Supercell	Mismatch on a	Mismatch on b
Al / Ph	4×1	1.9%	3.4%	5×1	1.3%	3.4%
Al / Ph-ox	4×1	2.4%	3.4%	5×1	1.8%	3.4%
Al ₂ O ₃ Al-term / Ph	3×2	2.3%	4.9%	2×1	1.9%	1.6%
Al ₂ O ₃ Al-term / Ph-ox	3×2	2.2%	4.3%	2×1	2.0%	2.1%
Al ₂ O ₃ O-term / Ph	3×2	0.1%	4.4%	2×1	4.2%	0.9%
Al ₂ O ₃ O-term / Ph-ox	3×2	0.3%	4.9%	2×1	4.6%	1.5%
Cu / Ph	5×1	3.1%	4.9%	7×1	3.0%	4.9%
Cu / Ph-ox	5×1	3.5%	4.9%	7×1	3.3%	4.9%
Cu ₂ O O-term / Ph	2×7	3.4%	1.1%	1×3	5.0%	2.3%
Cu ₂ O O-term / Ph-ox	2×7	3.0%	1.0%	1×3	5.0%	2.3%
Fe / Ph	6×2	0.2%	4.7%	5×3	0.3%	0.9%
Fe / Ph-ox	6×2	0.1%	2.6%	5×3	0.5%	1.3%
Fe ₂ O ₃ Fe-term / Ph	3×2	2.4%	1.0%	2×1	0.7%	0.3%
Fe ₂ O ₃ Fe-term / Ph-ox	3×2	2.6%	1.2%	2×1	0.5%	0.4%
Fe ₂ O ₃ O-term / Ph	3×2	2.3%	1.0%	2×1	0.7%	1.7%
Fe ₂ O ₃ O-term / Ph-ox	3×2	2.6%	1.2%	2×1	1.0%	1.9%
Cr / Ph	7×3	0.9%	4.4%	6×5	0.2%	2.1%
Cr / Ph-ox	7×3	0.4%	4.4%	6×5	0.8%	2.1%
Cr ₂ O ₃ Cr-term / Ph	3×2	2.9%	1.6%	2×1	0.8%	0.2%
Cr ₂ O ₃ Cr-term / Ph-ox	3×2	3.1%	1.8%	2×1	0.7%	0.4%

Table 2: Summary of constructed supercells for phosphorene-substrate interactions. Abbreviations: Ph: phosphorene, Ph-ox: oxidized phosphorene.

facilitating direct comparisons with Fe₂O₃ surface.

For the metal oxide substrates, different surface terminations were investigated by cleaving the structures along the z -axis to expose different outermost atomic layers. The notation used throughout this work indicates the chemical nature of the top-most layer: "Al-term" refers to an aluminum-terminated surface, "O-term" to an oxygen-terminated surface, "Fe-term" to an iron-terminated surface, "Cr-term" to a chromium-terminated surface, and "Cu-term" to a copper-terminated surface. The relaxed geometries of these different surface terminations are shown in the Supplementary Material.

After obtaining the optimized structures of the bulk and substrates, orthorhombic supercells were constructed by placing pristine and oxidized phosphorene above each of the substrates at different lateral positions, with an initial average distance of 2.0 Å. The most representative system chosen was the one with the lowest adhesion energy among the different lateral positions. The supercell was then relaxed according to the previously described criteria, maintaining a mismatch on the a and b vectors not exceeding 5% relative to the optimized vectors of the isolated systems.

Table 2 presents a summary of the constructed supercells, while the relaxed supercells for each system are shown in Figure 2.

The surface energy was calculated using Equation 1:

$$E_{\text{surface}} = \frac{E_{\text{sub}} - n \cdot E_{\text{bulk}}}{2A} \quad (1)$$

where E_{sub} and E_{bulk} are the total energies of the substrate and of the bulk, respectively, n is the ratio between the number of atoms in the substrate and in the bulk, and A is the area of the simulation cell. For phosphorene, the monolayer was considered for the calculation of E_{sub} .

The adhesion energy of pristine and oxidized phosphorene to the substrate was evaluated as:

$$E_{\text{adh}} = \frac{E_{\text{tot}} - E_{\text{ph}} - E_{\text{sub}}}{A} \quad (2)$$

where E_{tot} is the energy of the whole system, while E_{ph} and E_{sub} are the energies of the isolated phosphorene and substrate, respectively, and A is the in-plane area of the supercell.

To quantify the structural differences between the interacting structures in the supercell and their isolated counterparts, the Root Mean Square Deviation (RMSD) was employed through a custom Python script. RMSD is a widely adopted metric for expressing structural similarity by calculating the average deviation between equivalent atoms in two structures. While commonly used in protein structure analysis and MD simulations, it is also applicable in DFT studies [61, 62]. The RMSD is defined as:

$$\text{RMSD} = \sqrt{\frac{\sum_i d_i^2}{n}} \quad (3)$$

where d_i represents the distance between each of the n pairs of equivalent atoms in two optimally superimposed structures. The structures were aligned to minimize the effects of translation and rotation. An RMSD value of 0 Å indicates identical structures, with increasing values reflecting greater structural differences [63]. RMSD values are considered reliable indicators of variability when applied to highly similar structures, providing a quantitative measure of geometrical resemblance [63]. In this study, visual inspection of the phosphorene-substrate interactions revealed noticeable but not excessive distortions. Therefore, RMSD evaluation was considered an appropriate approximation for quantifying the degree of structural distortion.

To analyze the behavior of electronic charge resulting from the interaction between phosphorene and the substrate, the total electron charge redistribution per surface unit (Q_{red}) was computed by first subtracting the charge densities of the isolated components from the charge density of the combined system to obtain the charge density difference, $\Delta\rho(x, y, z)$. The resulting $\Delta\rho(x, y, z)$ was then integrated along the xy -plane to obtain the planar average charge density redistribution, $\Delta\rho(z)$. Finally, Q_{red} was obtained by integrating the absolute value of $\Delta\rho(z)$ along the z -axis and divided by the supercell area. This procedure was adapted from ref. [64].

To investigate the electronic structure of phosphorene, Projected Density of States (PDOS) calculations were performed using a denser K -points grid. The PDOS provide insights into the contributions of specific orbitals to the electronic states at each energy level, allowing for a detailed examination of the energy occupation around the Fermi level. In this study, the PDOS of the p orbitals in pristine and oxidized phosphorene were calculated and compared with that of the isolated structure.

3. Results and discussion

In order to determine the optimal structure of oxidized phosphorene, a series of calculations were performed. This involved placing an oxygen atom 1.5 Å away from each phosphorus atom and testing various configurations. Combinations of one- and two-sided oxygen adsorption were explored at different coverages (100%, 75%, 50%, and 25%). As reported in the literature [18], the most favorable configuration, exhibiting the lowest oxygen adsorption energy, corresponded to 25% coverage. A comparison between pristine and oxidized phosphorene is shown in Figure 1. It can be seen that the oxidized geometry exhibits greater distortion compared to the pristine structure, as evidenced by differences in bond lengths. Notably, as indicated in Table 1, oxidized phosphorene exhibits a lower surface energy compared to its pristine counterpart (0.12 J/m^2 and 0.18 J/m^2 , respectively). The higher stability of the oxidized form [65] aligns with experimental observations, which show that BP tends to oxidize spontaneously under ambient conditions [66].

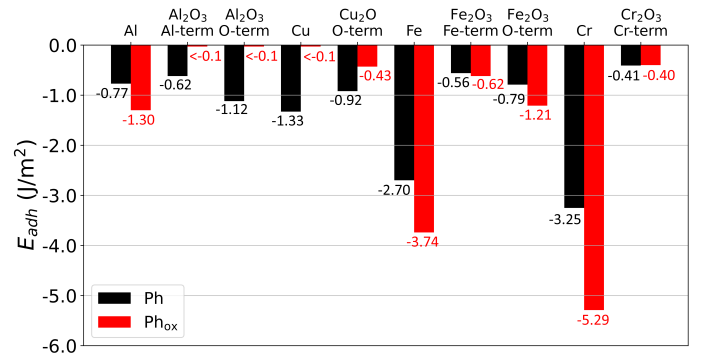


Figure 3: Adhesion energies for every phosphorene-substrate system.

The adhesion energies of pristine and oxidized phosphorene with various substrates were calculated to assess the strength of interaction, with the results presented in Figure 3. Overall, oxidized phosphorene exhibits slightly more favorable adhesion (more negative values) across all substrates. This could be attributed to the non-bonding states of the oxygen atoms, which can better interact with the empty states of the substrates. The adhesion to metallic surfaces of chromium and iron is particularly strong [21], especially for oxidized phosphorene. This enhanced interaction may be attributed to the partially filled 3d orbitals of Cr and Fe atoms, which are available to form bonds with both P and O atoms. In contrast, aluminum and copper show weaker adhesion, though still favorable. However, the interaction between copper and oxidized phosphorene is nearly negligible. These differences could be due to the different electronic configurations: Al has only one electron in the 3p orbital, while Cu has fully filled 3d orbitals, leading to different interactions with P and O atoms.

For oxide substrates, the adhesion energies are generally less favorable (less negative values) compared to their corresponding pristine metals. This can be attributed to the reduced availability of electronic charge for bonding, as oxides typically have fewer delocalized electrons than metals. Among the oxides, Fe₂O₃ shows the strongest adhesion, particularly with oxidized phosphorene and oxygen termination. Cu₂O exhibits better adhesion with pristine phosphorene, while Cr₂O₃ shows similar values for both forms. Notably, while Al₂O₃ demonstrates comparable adhesion to other oxides with pristine phosphorene, its interaction with oxidized phosphorene is extremely weak.

The relationship between the calculated adhesion energies and the experimental tribological performance reported in Ref. [16] reveals important insights.

In the experiments, the best results in terms of coefficient of friction (CoF) reduction were observed for scratched iron, where the superficial oxide layer was most likely removed, while non-scratched iron exhibited poor performance. This suggests that phosphorene-substrate adhesion plays a crucial role in enhancing the lubricating properties of BP, being significantly higher on pristine iron than on oxidized iron (Figure 3). This observation is consistent with findings for other layered materials used as solid lubricants, such as MXenes [67], and can be explained by considering that higher adhesion of the layers to the substrate prevents their peeling off during the rubbing process. Indeed, BP was found to reduce the CoF of non-scratched aluminum substrate only at the beginning of the tribological test, while after rubbing it reached the value measured for the unlubricated sample [16], in agreement with the low phosphorene-Al₂O₃ adhesion calculated in this work (Figure 3). The low phosphorene-

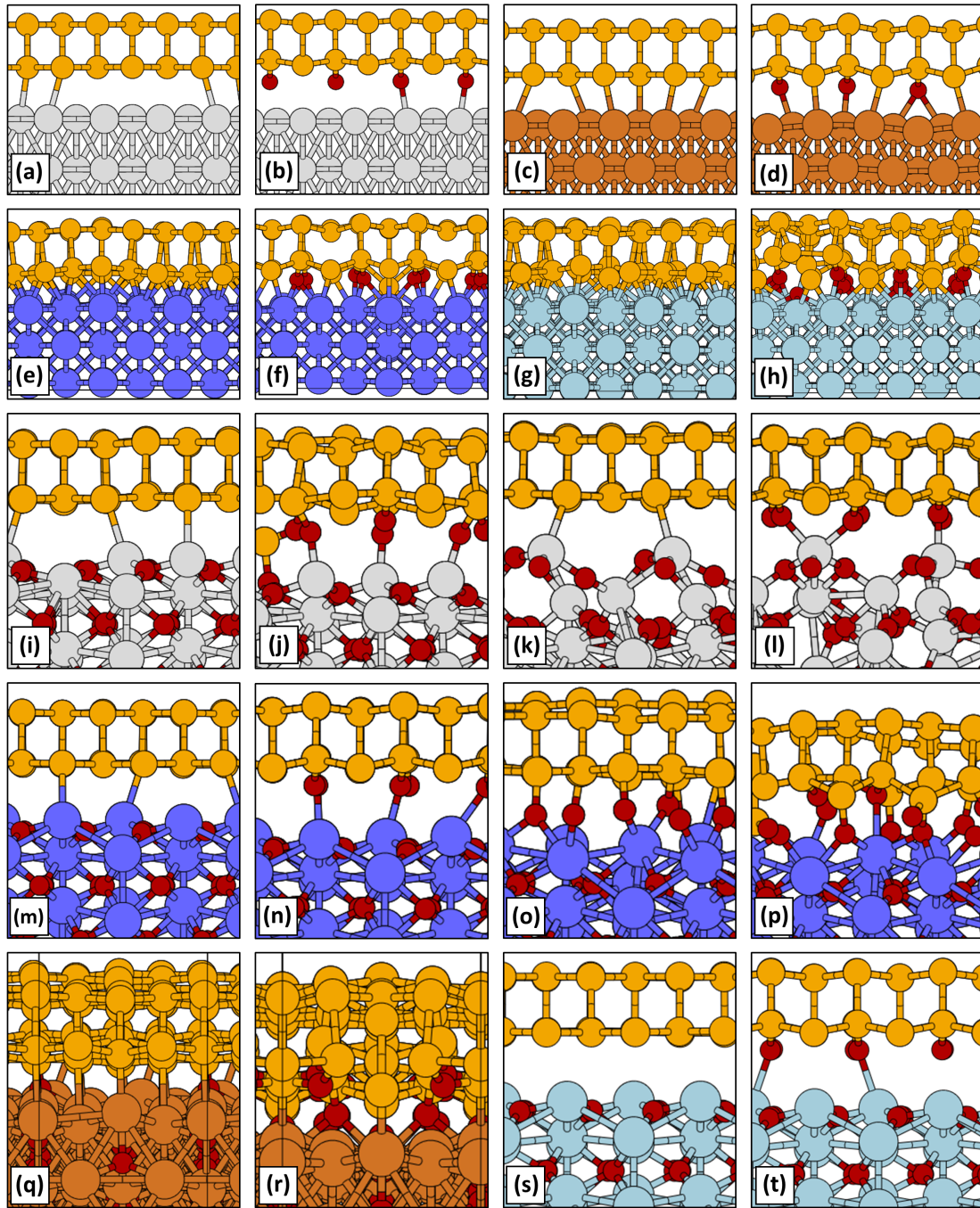


Figure 2: Relaxed geometries of the supercells: (a, b) pristine and oxidized phosphorene on aluminum, (c, d) pristine and oxidized phosphorene on copper, (e, f) pristine and oxidized phosphorene on iron, (g, h) pristine and oxidized phosphorene on chromium, (i, j) pristine and oxidized phosphorene on Al_2O_3 Al-terminated, (k, l) pristine and oxidized phosphorene on Al_2O_3 O-terminated, (m, n) pristine and oxidized phosphorene on Fe_2O_3 Fe-terminated, (o, p) pristine and oxidized phosphorene on Fe_2O_3 O-terminated, (q, r) pristine and oxidized phosphorene on Cu_2O O-terminated, (s, t) pristine and oxidized phosphorene on Cr_2O_3 Cr-terminated. Color code: P atoms are shown in yellow, Al in grey, Fe in purple, Cu in orange, Cr in cyan, and O in red.

Cu_2O adhesion may suggest an irrelevant effect of BP in reducing the CoF of copper, as observed for aluminum. However, the experimental results indicate an even worse effect of BP on copper, which was interpreted as third-body wear effect due to the poor adhesion.

Figure 4 presents the evaluation of RMSD for phosphorene-substrate interactions. Analysis of the data reveals a weak correlation between RMSD values and adhesion energies. In general, oxidized phosphorene exhibits higher RMSD values compared to its pristine counterpart, aligning with its more favorable adhesion energies. This suggests that oxidized phosphorene undergoes greater structural distortion due to the more favorable in-

teraction. However, the pattern of increased distortion observed for oxidized phosphorene does not extend to the corresponding substrate surfaces. This observation implies that the structural changes are predominantly confined to the phosphorene layer, with minimal deformation occurring in the substrate materials. Notably, Cu_2O stands as an exception to this trend.

Figure 5 presents the overall assessment of charge redistribution (Q_{red}) when phosphorene is deposited on the substrate. In agreement with previous studies [21, 64], higher interfacial adhesion (i.e., more negative adhesion energies) is associated with higher Q_{red} values. Moreover, Q_{red} follows the same trend as adhesion, increasing from Al to Cu, Fe, and Cr in the case of

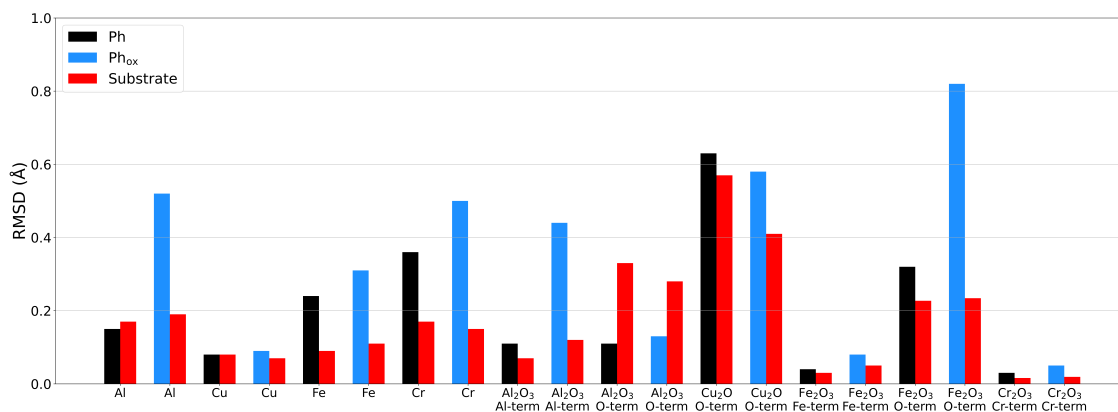


Figure 4: RMSD analysis for every phosphorene-substrate system.

pristine metals, while it remains very low for oxides, except for O-terminated Fe₂O₃, where the adhesion is higher than for the other oxides.

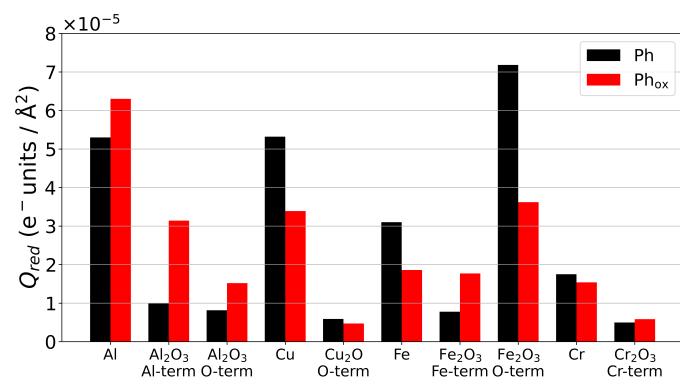


Figure 5: Total electron charge redistribution per surface unit (Q_{red}) for every phosphorene-substrate system.

Figures 6 and 7 illustrate the charge analysis, specifically $\Delta\rho(z)$ and PDOS. As shown in these figures, Q_{red} is higher for pristine metals than for their oxidized counterparts. This may be attributed to the fact that pristine metals, with less localized charge compared to metal oxides, have more surface dangling bonds and can more easily form new bonds with phosphorene, increasing the charge redistribution.

Regarding $\Delta\rho(z)$, which does not necessarily correlate with Q_{red} due to its dependence on the supercell area, a greater charge redistribution is generally observed in pristine metals compared to their respective oxides. Overall, charge accumulation is noted in the interfacial region, attributed to the formation of new bonds between phosphorene and the substrate surface.

From the PDOS analysis, an increase in phosphorene p -states within the band gap is observed in some cases after interaction with the substrate (e.g., Figures 6(j) and 6(l)). In these cases, phosphorene exhibits metallic character [68]. In some instances, metallic behavior emerges only for oxidized phosphorene (e.g., Figures 6(b) and 6(d)), whereas in other cases it is observed for both pristine and oxidized phosphorene (e.g., Figures 6(j) and 6(l)). Conversely, in some systems no p -states appear within the band gap (e.g., Figures 6(b) and 7(b)), thus preserving the insulating character. Moreover, no strong correlation is found between the emergence of metallic behavior in phosphorene and the Q_{red} values, as evidenced by the comparison between Figures 6(j) and 6(l) and the Q_{red} value reported for Cr in Figure

5.

4. Conclusion

DFT calculations were performed to determine the adhesion energy of both pristine and oxidized phosphorene on different pristine and oxidized metallic substrates. The results demonstrate that oxidized phosphorene generally exhibits higher adhesion to all substrates compared to its pristine counterpart. This enhanced adhesion can be attributed to more favorable interactions between the non-bonding states of oxygen atoms and the empty electronic states of the substrates.

The RMSD structural analysis revealed that oxidized phosphorene exhibits higher structural distortion values, consistent with its more favorable adhesion to substrates. Phosphorene adhesion is consistently more favorable on pristine metal surfaces than on their oxidized counterparts. This difference stems from the reduced availability of electronic charge for bonding in metal oxides, due to increased localization within the oxide structure.

Comparison of the calculated adhesion energies with experimental tribological results [16] reveals that stronger adhesion (i.e., more negative energy values) correlates with reduced CoF. Consistently, the nearly negligible effect of BP on aluminum, copper, iron, and steel samples agrees with the low adhesion predicted for phosphorene on oxidized metal surfaces. In contrast, removing the oxide layer by scratching the iron sample prior to tribological testing resulted in a decrease in CoF, in line with the higher adhesion calculated for pristine iron compared to its oxidized form.

The charge redistribution analysis (Q_{red}) demonstrated that greater charge redistribution generally occurs with pristine metals compared to their respective oxides, consistent with the observed adhesion energy trends. The PDOS analysis revealed that strong interaction with the substrate, such as with pristine iron and chromium surfaces, leads to the filling of phosphorene p -states within the band gap, transforming its character from semi-conducting to metallic.

The present computational work provides fundamental insights into the substrate-dependent tribological performance of BP by establishing quantitative relationships between interfacial adhesion energies and experimentally observed friction behavior, demonstrating that layer-substrate adhesion is a key factor governing the effectiveness of BP as a solid lubricant.

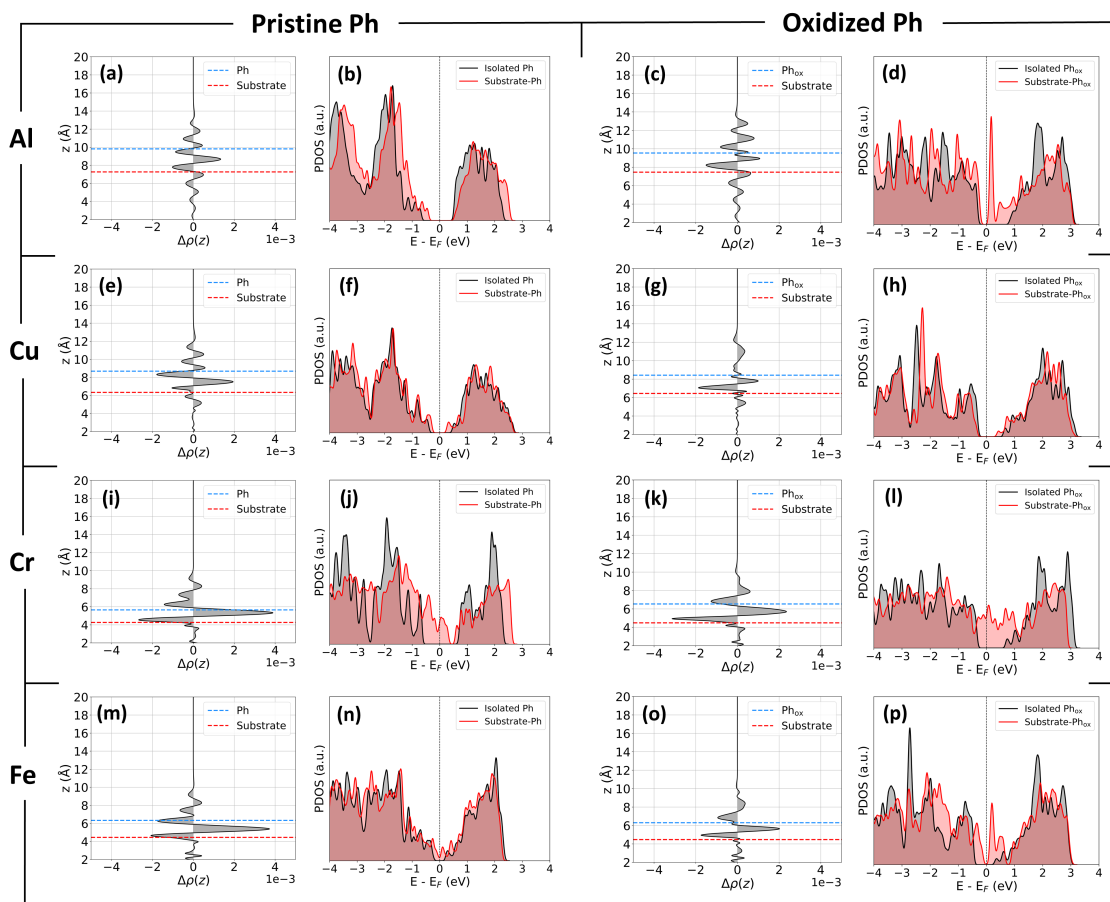


Figure 6: $\Delta\rho(z)$ and PDOS analysis for every phosphorene-substrate system.

CRedit authorship contribution statement

Matteo Vezzelli: Writing - Review & Editing, Writing - original draft, Visualization, Validation, Investigation, Formal analysis, Conceptualization. **Carsten Gachot:** Review & Editing, Conceptualization. **Maria Clelia Righi:** Writing - Review & Editing, Conceptualization, Supervision, Funding acquisition.

Declaration of competing interest

The authors declare that they have no known competing financial interests or personal relationships that could have appeared to influence the work reported in this paper.

Data availability

Data will be made available on request.

Acknowledgements

These results are part of the project “Advancing Solid Interface and Lubricants by First Principles Material Design (SLIDE)” that has received funding from the European Research Council (ERC) under the Horizon 2020 Research and Innovation program of the European Union (Grant agreement No. 865633). Furthermore, we acknowledge the CINECA award under the IS-CRA initiative, for the availability of high-performance computing resources and support.

References

- [1] X. Ling, H. Wang, S. Huang, F. Xia, M. S. Dresselhaus, The renaissance of black phosphorus, *Proceedings of the National Academy of Sciences* 112 (15) (2015) 4523–4530.
- [2] E. Marquis, M. Cutini, B. Anasori, A. Rosenkranz, M. C. Righi, Nanoscale mxene interlayer and substrate adhesion for lubrication: a density functional theory study, *ACS Applied Nano Materials* 5 (8) (2022) 10516–10527.
- [3] L. Kou, C. Chen, S. C. Smith, Phosphorene: fabrication, properties, and applications, *The journal of physical chemistry letters* 6 (14) (2015) 2794–2805.
- [4] A. Carvalho, M. Wang, X. Zhu, A. S. Rodin, H. Su, A. H. Castro Neto, Phosphorene: from theory to applications, *Nature Reviews Materials* 1 (11) (2016) 1–16.
- [5] T. Low, A. Rodin, A. Carvalho, Y. Jiang, H. Wang, F. Xia, A. Castro Neto, Tunable optical properties of multilayer black phosphorus thin films, *Physical Review B* 90 (7) (2014) 075434.
- [6] A. Rodin, A. Carvalho, A. Castro Neto, Strain-induced gap modification in black phosphorus, *Physical review letters* 112 (17) (2014) 176801.
- [7] J. Tao, W. Shen, S. Wu, L. Liu, Z. Feng, C. Wang, C. Hu, P. Yao, H. Zhang, W. Pang, et al., Mechanical and electrical anisotropy of few-layer black phosphorus, *ACS nano* 9 (11) (2015) 11362–11370.

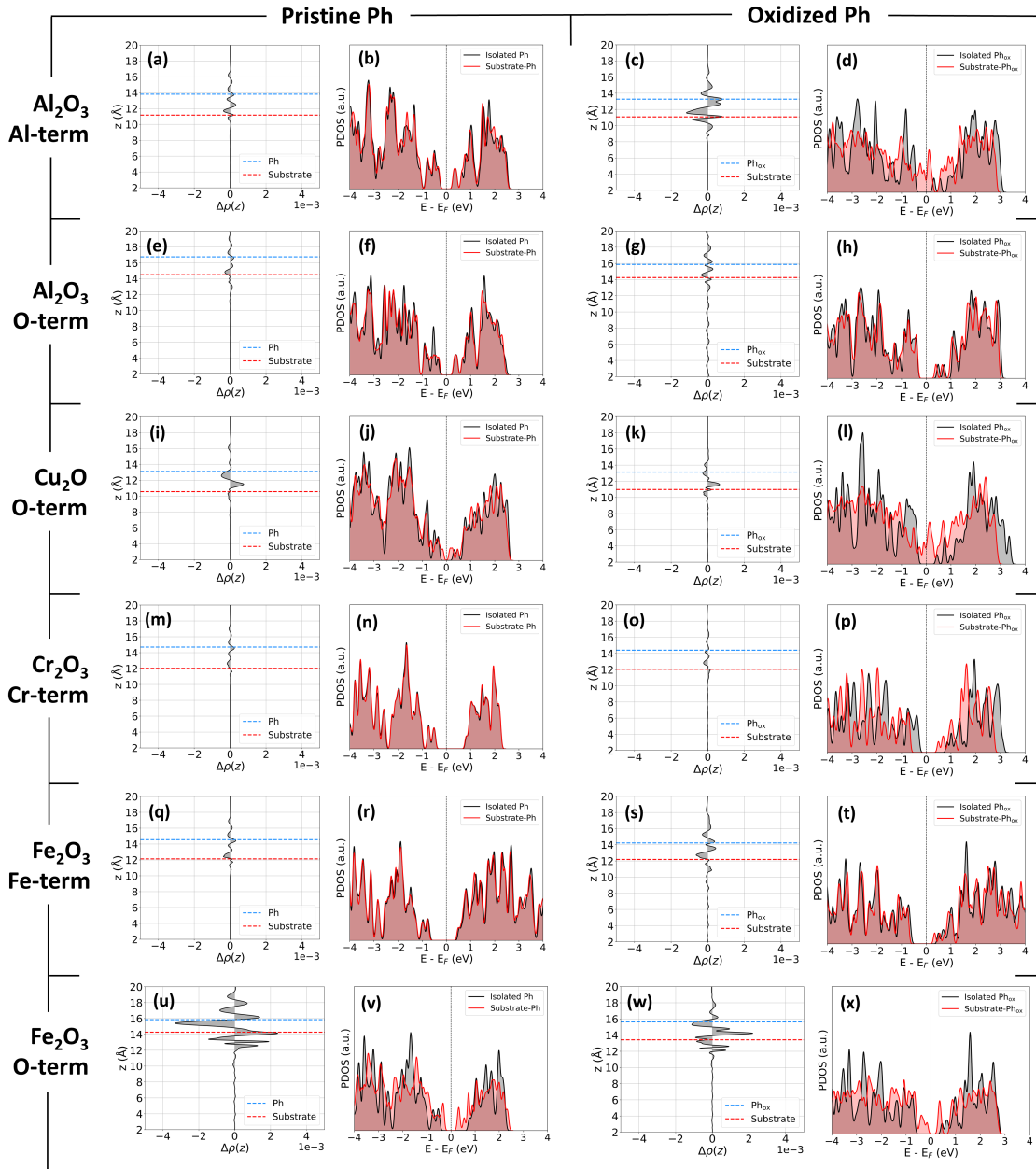


Figure 7: $\Delta\rho(z)$ and PDOS analysis for every phosphorene-substrate system.

- [8] W. Wang, G. Xie, J. Luo, Superlubricity of black phosphorus as lubricant additive, *ACS Applied Materials & Interfaces* 10 (49) (2018) 43203–43210.
- [9] Z. Cui, G. Xie, F. He, W. Wang, D. Guo, W. Wang, Atomic-scale friction of black phosphorus: effect of thickness and anisotropic behavior, *Advanced Materials Interfaces* 4 (23) (2017) 1700998.
- [10] Y. Lv, W. Wang, G. Xie, J. Luo, Self-lubricating ptfе-based composites with black phosphorus nanosheets, *Tribology Letters* 66 (2) (2018) 61.
- [11] W. Wang, G. Xie, J. Luo, Black phosphorus as a new lubricant, *Friction* 6 (1) (2018) 116–142.
- [12] P. Restuccia, M. C. Righi, Tribochemistry of graphene on iron and its possible role in lubrication of steel, *Carbon* 106 (2016) 118–124.
- [13] D. Marchetto, P. Restuccia, A. Ballestrazzi, M. C. Righi, A. Rota, S. Valeri, Surface passivation by graphene in the lubrication of iron: A comparison with bronze, *Carbon* 116 (2017) 375–380.
- [14] D. Philippon, M.-I. de Barros-Bouchet, T. Mogne, E. Gresser, J.-M. Martin, Experimental simulation of phosphites additives tribochemical reactions by gas phase lubrication, *Tribology-Materials, Surfaces & Interfaces* 1 (3) (2007) 113–123.
- [15] M. De Barros-Bouchet, M. C. Righi, D. Philippon, S. Mamingo-Doumbe, T. Le-Mogne, J. Martin, A. Bouffet, Tribochemistry of phosphorus additives: experiments and first-principles calculations, *Rsc Advances* 5 (61) (2015) 49270–49279.
- [16] M. Vezzelli, M. Rodríguez Ripoll, S. Schwarz, A. Erdemir, M. C. Righi, C. Gachot, A different perspective on the solid

- lubrication performance of black phosphorous: Friend or foe?, *Advanced Engineering Materials* (2024) 2401756.
- [17] G. Losi, P. Restuccia, M. Righi, Superlubricity in phosphorene identified by means of ab initio calculations, *2D Materials* 7 (2) (2020) 025033.
- [18] F. Benini, N. Bassoli, P. Restuccia, M. Ferrario, M. C. Righi, Interaction of water and oxygen molecules with phosphorene: an ab initio study, *Molecules* 28 (8) (2023) 3570.
- [19] H. Zhang, N. M. Abbasi, B. Wang, *Semiconducting Black Phosphorus: From 2D Nanomaterial to Emerging 3D Architecture*, CRC Press, 2021.
- [20] R. Boddula, A. M. Asiri, *Black Phosphorus*, Springer, 2020.
- [21] G. Losi, M. Cutini, P. Restuccia, M. C. Righi, Modeling phosphorene and mos 2 interacting with iron: lubricating effects compared to graphene, *Journal of Nanostructure in Chemistry* 13 (5) (2023) 497–505.
- [22] G. Abellan, S. Wild, V. Lloret, N. Scheuschner, R. Gillen, U. Mundloch, J. Maultzsch, M. Varela, F. Hauke, A. Hirsch, Fundamental insights into the degradation and stabilization of thin layer black phosphorus, *Journal of the American Chemical Society* 139 (30) (2017) 10432–10440.
- [23] J. O. Island, G. A. Steele, H. S. van der Zant, A. Castellanos-Gomez, Environmental instability of few-layer black phosphorus, *2D Materials* 2 (1) (2015) 011002.
- [24] K. L. Kuntz, R. A. Wells, J. Hu, T. Yang, B. Dong, H. Guo, A. H. Woomer, D. L. Druffel, A. Alabanza, D. Tománek, et al., Control of surface and edge oxidation on phosphorene, *ACS applied materials & interfaces* 9 (10) (2017) 9126–9135.
- [25] A. Favron, E. Gaufrès, F. Fossard, A.-L. Phaneuf-L'Heureux, N. Y. Tang, P. L. Lévesque, A. Loiseau, R. Leonelli, S. Francoeur, R. Martel, Photooxidation and quantum confinement effects in exfoliated black phosphorus, *Nature materials* 14 (8) (2015) 826–832.
- [26] W. Luo, D. Y. Zemlyanov, C. A. Milligan, Y. Du, L. Yang, Y. Wu, P. D. Ye, Surface chemistry of black phosphorus under a controlled oxidative environment, *Nanotechnology* 27 (43) (2016) 434002.
- [27] Z. Hu, Q. Li, B. Lei, Q. Zhou, D. Xiang, Z. Lyu, F. Hu, J. Wang, Y. Ren, R. Guo, et al., Water-catalyzed oxidation of few-layer black phosphorous in a dark environment, *Angewandte Chemie International Edition* 56 (31) (2017) 9131–9135.
- [28] Q. Zhou, Q. Chen, Y. Tong, J. Wang, Light-induced ambient degradation of few-layer black phosphorus: mechanism and protection, *Angewandte Chemie International Edition* 55 (38) (2016) 11437–11441.
- [29] Y. Huang, J. Qiao, K. He, S. Bliznakov, E. Sutter, X. Chen, D. Luo, F. Meng, D. Su, J. Decker, et al., Interaction of black phosphorus with oxygen and water, *Chemistry of Materials* 28 (22) (2016) 8330–8339.
- [30] S. Wu, F. He, G. Xie, Z. Bian, J. Luo, S. Wen, Black phosphorus: Degradation favors lubrication, *Nano letters* 18 (9) (2018) 5618–5627.
- [31] Z. Wang, L. Zhu, G. Xie, X. Ren, Effect of black phosphorus oxidation on tribological properties of polytetrafluoroethylene-based composites, *Journal of Materials Engineering and Performance* 31 (12) (2022) 9972–9984.
- [32] A. H. Jayatissa, B. R. Manu, Tribological properties at the interface of the aluminum and aluminum oxide, *methods* 5 (5) (2019).
- [33] S. Ali, G. Wood, Oxidation of iron at room temperature, *British Corrosion Journal* 4 (3) (1969) 133–137.
- [34] W. Vernon, E. Calnan, C. B. Clews, T. Nurse, The oxidation of iron around 200 c, *Proceedings of the Royal Society of London. Series A. Mathematical and Physical Sciences* 216 (1126) (1953) 375–397.
- [35] D. Davies, U. R. Evans, J. Agar, The oxidation of iron at 175 to 350 c, *Proceedings of the Royal Society of London. Series A. Mathematical and Physical Sciences* 225 (1163) (1954) 443–462.
- [36] X. Huang, S. K. Ramadugu, S. E. Mason, Surface-specific dft+ u approach applied to α -fe₂o₃ (0001), *The Journal of Physical Chemistry C* 120 (9) (2016) 4919–4930.
- [37] S.-K. Lee, H.-C. Hsu, W.-H. Tuan, Oxidation behavior of copper at a temperature below 300 c and the methodology for passivation, *Materials Research* 19 (1) (2016) 51–56.
- [38] N. Greenwood, A. Earnshaw, *Chemistry of the elements* 2nd Edition, Butterworth-Heinemann, 1997.
- [39] B. Cho, E. Choi, S. Chung, K. Kim, T. Kang, C. Park, B. Kim, A novel cr₂o₃ thin film on stainless steel with high sorption resistance, *Surface science* 439 (1-3) (1999) L799–L802.
- [40] X. Huang, D. Costa, B. Diawara, V. Maurice, P. Marcus, Atomistic insights on enhanced passivity: Dft study of substitutional mo on cr₂o₃ and fe₂o₃ surfaces, *Corrosion Science* 224 (2023) 111543.
- [41] P. Giannozzi, S. Baroni, N. Bonini, M. Calandra, R. Car, C. Cavazzoni, D. Ceresoli, G. L. Chiarotti, M. Cococcioni, I. Dabo, et al., Quantum espresso: a modular and open-source software project for quantum simulations of materials, *Journal of physics: Condensed matter* 21 (39) (2009) 395502.
- [42] D. Vanderbilt, Soft self-consistent pseudopotentials in a generalized eigenvalue formalism, *Physical review B* 41 (11) (1990) 7892.
- [43] J. P. Perdew, K. Burke, M. Ernzerhof, Generalized gradient approximation made simple, *Physical review letters* 77 (18) (1996) 3865.
- [44] D. F. Shanno, Conditioning of quasi-newton methods for function minimization, *Mathematics of computation* 24 (111) (1970) 647–656.

- [45] S. Grimme, Semiempirical gga-type density functional constructed with a long-range dispersion correction, *Journal of computational chemistry* 27 (15) (2006) 1787–1799.
- [46] L. Shulenburger, A. D. Baczewski, Z. Zhu, J. Guan, D. Tomanek, The nature of the interlayer interaction in bulk and few-layer phosphorus, *Nano letters* 15 (12) (2015) 8170–8175.
- [47] N. Naveas, R. Pulido, C. Marini, P. Gargiani, J. Hernandez-Montelongo, I. Brito, M. Manso-Silvan, First-principles calculations of magnetite (Fe₃O₄) above the Verwey temperature by using self-consistent DFT+U+V, *Journal of Chemical Theory and Computation* 19 (23) (2023) 8610–8623.
- [48] S. C. Dhanabalan, J. S. Ponraj, Z. Guo, S. Li, Q. Bao, H. Zhang, Emerging trends in phosphorene fabrication towards next generation devices, *Advanced Science* 4 (6) (2017) 1600305.
- [49] A. Jain, S. P. Ong, G. Hautier, W. Chen, W. D. Richards, S. Dacek, S. Cholia, D. Gunter, D. Skinner, G. Ceder, et al., Commentary: The materials project: A materials genome approach to accelerating materials innovation, *APL materials* 1 (1) (2013).
- [50] A. Kiejna, B. I. Lundqvist, First-principles study of surface and subsurface O structures at Al(111), *Physical Review B* 63 (8) (2001) 085405.
- [51] L. Vitos, A. V. Ruban, H. L. Skriver, J. Kollar, The surface energy of metals, *Surface Science* 411 (1-2) (1998) 186–202.
- [52] H.-N. Chiang, S. Nachimuthu, Y.-C. Cheng, N. P. Damayanti, J.-C. Jiang, A DFT study of ethanol adsorption and decomposition on α -Al₂O₃(0001) surface, *Applied Surface Science* 363 (2016) 636–643.
- [53] B. Ramogayana, D. Santos-Carballal, K. P. Maenetja, N. H. De Leeuw, P. E. Ngoepe, Density functional theory study of ethylene carbonate adsorption on the (0001) surface of aluminum oxide α -Al₂O₃, *ACS Omega* 6 (44) (2021) 29577–29587.
- [54] J. Sun, T. Stirner, A. Matthews, Structure and surface energy of low-index surfaces of stoichiometric α -Al₂O₃ and α -Cr₂O₃, *Surface and Coatings Technology* 201 (7) (2006) 4205–4208.
- [55] R. Zhang, L. Li, L. Frazer, K. B. Chang, K. R. Poepelmeier, M. K. Chan, J. R. Guest, Atomistic determination of the surface structure of Cu₂O(111): Experiment and theory, *Physical Chemistry Chemical Physics* 20 (43) (2018) 27456–27463.
- [56] A. Kokalj, S. Peljhan, Density functional theory study of adsorption of benzotriazole on Cu₂O surfaces, *The Journal of Physical Chemistry C* 119 (21) (2015) 11625–11635.
- [57] Y. Gao, L. Zhang, A. J. van Hoof, E. J. Hensen, On the surface-dependent oxidation of Cu₂O during CO oxidation: Cu²⁺ is more active than Cu⁺, *Applied Catalysis A: General* 602 (2020) 117712.
- [58] M.-T. Nguyen, N. Seriani, R. Gebauer, Water adsorption and dissociation on α -Fe₂O₃(0001): PBE+U calculations, *The Journal of chemical physics* 138 (19) (2013).
- [59] A. Rohrbach, J. Hafner, G. Kresse, Ab initio study of the (0001) surfaces of hematite and chromia: Influence of strong electronic correlations, *Physical Review B—Condensed Matter and Materials Physics* 70 (12) (2004) 125426.
- [60] D. Costa, K. Sharkas, M. M. Islam, P. Marcus, Ab initio study of the chemical states of water on Cr₂O₃(0001): From the isolated molecule to saturation coverage, *Surface Science* 603 (16) (2009) 2484–2493.
- [61] L. M. Debever, C. J. Pollock, Systematic assessment of DFT methods for geometry optimization of mononuclear platinum-containing complexes, *Physical Chemistry Chemical Physics* 23 (43) (2021) 24780–24788.
- [62] A. Sharma, G. Ohanessian, C. Clavaguera, Accuracy of density functionals in the description of dispersion interactions and IR spectra of phosphates and phosphorylated compounds, *Journal of molecular modeling* 20 (9) (2014) 2426.
- [63] O. Carugo, S. Pongor, A normalized root-mean-square distance for comparing protein three-dimensional structures, *Protein Science* 10 (7) (2001) 1470–1473.
- [64] M. Wolloch, G. Levita, P. Restuccia, M. Righi, Interfacial charge density and its connection to adhesion and frictional forces, *Physical Review Letters* 121 (2) (2018) 026804.
- [65] R. Tran, Z. Xu, B. Radhakrishnan, D. Winston, W. Sun, K. A. Persson, S. P. Ong, Surface energies of elemental crystals, *Scientific Data* 3 (1) (2016) 1–13.
- [66] Q. Zhong, X. Pang, Exploring the oxidation mechanisms of black phosphorus: a review, *Journal of Materials Science* 58 (5) (2023) 2068–2086.
- [67] E. Marquis, D. Lizama, R. Espinoza-Gonzalez, A. Rosenkranz, M. C. Righi, MXene-substrate adhesion-towards more efficient and durable coatings, *Materials Today Nano* (2025) 100705.
- [68] Y. Pan, Y. Wang, M. Ye, R. Quhe, H. Zhong, Z. Song, X. Peng, D. Yu, J. Yang, J. Shi, et al., Monolayer phosphorene–metal contacts, *Chemistry of Materials* 28 (7) (2016) 2100–2109.